

## Direct CO<sub>2</sub>-to-dimethyl Ether Hydrogenation over CuZnZr/zeolite Hybrid Catalyst: New Evidences on the Interaction Between Acid and Metal Sites

Enrico Catizzone<sup>1\*</sup>, Giuseppe Bonura<sup>2</sup>, Massimo Migliori<sup>3</sup>, Giacobbe Braccio<sup>1</sup>, Francesco Frusteri<sup>2</sup>, Girolamo Giordano<sup>3</sup>

<sup>1</sup> ENEA-Italian National Agency for New Technologies, Energy and Sustainable Economic Development, Trisaia Research Centre, Rotondella 75026, Italy

<sup>2</sup> CNR-ITAE, Istituto di Tecnologie Avanzate per l'Energia "Nicola Giordano", via S. Lucia Sopra Contesse, 5, Messina 98126, Italy

<sup>3</sup> Department of Environmental and Chemical Engineering, University of Calabria, via P. Bucci, 44a, Rende 87036, Italy

Corresponding Author Email: [enrico.catizzone@enea.it](mailto:enrico.catizzone@enea.it)

<https://doi.org/10.18280/acsm.430302>

**Received:** 5 March 2019

**Accepted:** 20 May 2019

### Keywords:

CO<sub>2</sub> recycling, dimethyl ether, heterogeneous catalysis, zeolites, nanostructured catalysts, Lewis/Brønsted acid sites, industrial chemistry processes

### ABSTRACT

The production of DME via one-pot CO<sub>2</sub> hydrogenation is a strategic way of recycling CO<sub>2</sub> with the production of a high-value added product. This work aims to investigate the effect of the main zeolite features, e.g. structure or acidity, on the activity, selectivity and stability of the catalyst for DME production via both methanol dehydration and one-pot CO<sub>2</sub> hydrogenation. Several zeolites (i.e. FER and MFI) were synthesized and deeply characterized with XRD, B.E.T, NH<sub>3</sub>-TPD and FTIR. Obtained crystals were used as catalysts for methanol dehydration as well as for one-pot CO<sub>2</sub>-to-DME process. Obtained results allow giving new insights about the role of the interaction between metals and acid sites for an efficient DME production via one-pot CO<sub>2</sub> hydrogenation. In particular, zeolite acidity plays a crucial role in methanol dehydration step and Lewis acid sites seems to be more active than Brønsted sites. Furthermore, metal/acid proximity plays a key factor in one-pot CO<sub>2</sub> hydrogenation; in fact, the catalytic performances of multifunctional catalytic bed improve by increasing the metal/acid sites proximity. The findings of this research allow to highlight the main factors to be taken into account in terms of design and optimization of new catalytic systems for DME synthesis.

## 1. INTRODUCTION

The continue grow of the world's population and the rapid development of emerging economies cause require in import increase in the worldwide demand of energy. With the ever-growing concern on world environmental pollution the quest for cleaner energy sources is strengthened in order to minimize the impact on the environment. Nowadays, natural gas valorisation represents a reliable way to overtake the other fossil fuel in terms of availability, accessibility, versatility, low cost and a smaller environmental footprint. In this sense, The International Energy Agency (IEA) has estimated that the global demand of natural gas could rise could be set to grow more than 50 % by 2035, from 2010 levels, especially if gas natural extraction, by both conventional or unconventional route (e.g. shale gas), is joined with a right valorisation of this raw material [1-2]. Production of syngas (mixture of H<sub>2</sub>, CO and CO<sub>2</sub>) by partial oxidation, steam reforming or autothermic treatment of methane or natural gas, represents a highly efficient way to valorise these energy sources with production high value products [3-4]. Indeed, environmental and economic sustainability of important syngas-based industrial processes, as Fischer-Tropsch, Methanol-to-Gasoline, Methanol-to-Olefins and ammonia process, is strongly affected by syngas production system. Furthermore, the production of syngas from biomass gasification is a reliable alternative route to strongly increase the sustainability of above-mentioned

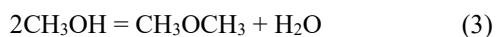
industrial processes [5-6]. Environmental impact during the utilization of the final product is also an important challenge of modern both academic and industrial research in order to increase sustainability of these energetic sources. In this concern, production of dimethyl ether (DME) from natural gas or biomass permits to obtain an alternative Diesel fuel with a high well-to-wheel efficiency compared with other fuel (i.e. methane, ethanol, and Fisher-Tropsch fuels) and, according with the above mentioned economic and environmental aspects, it represents a reliable alternative fuel with very high sustainability [7]. DME has received a growing attention as sustainable alternative fuel for Diesel engines because to its high cetane number (>55) and to the important reduction of NO<sub>x</sub> emissions and total absence of SO<sub>x</sub> and particulate matter in flue gases [8], unlike when diesel fuel is used. DME (CH<sub>3</sub> – O – CH<sub>3</sub>), the simplest of the ethers, is a colourless, non-toxic, non-corrosive, non-carcinogenic and environmentally friendly compound with a normal boiling point of -25 °C that can be liquefied above 0.5 MPa at room temperature. Furthermore, DME has chemical and physical properties similar to those of propane and butane, the main constituents of LPG, so it could be distributed, stored and utilized as an LPG substitute without increase of costs [9]. DME can be industrially synthesized in two routes following the indirect or direct synthesis. Indirect synthesis is a two-steps process: the traditional methanol synthesis from syngas (H<sub>2</sub>-CO ratio equals to about 2) over Cu/ZnO/Al<sub>2</sub>O<sub>3</sub> (CZA) redox catalyst, in the temperature

range 240-280 °C and pressure between 3 and 7 MPa [10], followed by methanol dehydration reaction to dimethyl ether over an acid catalyst. On the other hand, the direct synthesis is a one-step process where the two reactions, methanol synthesis (via CO hydrogenation) and the dehydration to DME, take place in the same reactor under process conditions close to those of methanol synthesis [10]. The one-step route is more efficient than double-step one, mainly because of the thermodynamic advantages in case of simultaneous reactions (with concerted methanol dehydration is possible to increase the extent of reaction of syngas-to-alcohol step) but also for the lower processing costs. Valorisation and reusing of carbon dioxide emitted from power station in an important challenge in order to mitigate the growing global warming [11-20]. In this sense, a growing attention is receiving the synthesis of methanol or DME by total or partial substitution of CO with CO<sub>2</sub>.

In particular, in the one-pot CO<sub>2</sub> hydrogenation process, the DME synthesis net reaction is given by the reaction reported in Eq. (1):

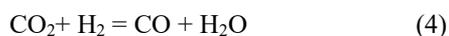


involving the carbon dioxide hydrogenation to methanol, Eq. (2), and methanol dehydration, Eq. (3).



DME synthesis reaction is an exothermic reaction that releases about 122 kJ of heat for each DME mol produced. For this reason, from a thermodynamic point of view, a decrease in reaction temperature should favor the synthesis of DME.

Furthermore, high pressure also should favor DME production since the reaction occurs with a reduction of total moles number [15]. Nevertheless, temperatures above 240 °C are usually requested for facilitating CO<sub>2</sub> activation rate since CO<sub>2</sub> is not a highly reactive molecule. On the other side, high reaction temperature favors endothermic side reactions such as reverse water gas shift that consume carbon dioxide and hydrogen producing carbon monoxide and water as reported in Eq. (4):



Furthermore, hydrocarbons and coke may be formed during such process. The deposition of coke on catalyst surface is well-known cause of deactivation.

Therefore, highly active and selective catalyst is required to avoid the formation of undesired by-product. Anyhow, irrespective of the process applied for the DME synthesis, it has been demonstrated that the properties of the acid matrix significantly affect selectivity and durability of bi-functional catalyst as well as the overall process efficiency, being controlled by the dehydration step [21-22].

Several studies have been carried out using  $\gamma$ -Al<sub>2</sub>O<sub>3</sub> as acid catalyst reporting high selectivity towards DME formation in the temperature range 200-300 °C, but also rapid deactivation by water adsorption on Lewis acid sites, especially during the direct synthesis via CO<sub>2</sub> hydrogenation where a lot amount of water is formed from both methanol dehydration and reverse-water-gas-shift reaction [23]. So, a more hydrophobic acid

catalyst is suggested to be used in this gas-to-liquid reaction. As alternative to  $\gamma$ -Al<sub>2</sub>O<sub>3</sub>, zeolites have been also investigated revealing a better stability to water and higher methanol conversion [24-28].

Activity, selectivity and stability of zeolites applied in acid-catalysed reactions are recognised to depend upon several factors as zeolite structure, acidity and crystal size. Zeolite channel system (channel orientation and opening size) is a well-known factor affecting strongly products distribution and catalyst deactivation [29-38].

Zeolite deactivation in both DME or olefins synthesis is due mainly to coke deposition and catalyst structure and acidity affect strongly mechanism of coke formation and the effect of coke on behaviour of the catalyst overtime. Campelo et al. [39] report a comparison between several silico-aluminophosphate with different channel configuration (1-, 2- and 3-dimensional) and it is showed that on a 3-dimensional structure (as SAPO-34), the oligomers formed in the channel can migrate to the big cage of this structure where react over strong acid sites leading formation of heavier oligomers and aromatics that cannot back to the channel causing a rapid catalyst deactivation for pore blocking. On the other hand, deactivation of 1-dimensional large channel (as SAPO-5) is due to the adsorption of multi branched chains on the strong acid sites causing blocking of the pore system. Structures with both small/medium channels and cages, as MFI type, don't permit trapping of heavy compounds inside the crystal and coke is preferably formed on external surface of crystals and catalyst deactivation occurs by coke deposition on the mouth of the channels [29, 37]. Catalyst deactivation rate is also affected from crystal morphology: small or hierarchical crystals exhibits higher resistance to deactivation by coke deposition than large crystal with microporous textural [34-35]. On small 1-D structures, as MTF, no hydrocarbon pool mechanisms are observed even at high temperature (400 °C) and DME is the only product detected in reactor outstream; nevertheless, this structure exhibits fast deactivation over time [45]. In order to produce DME catalyst structure is a key parameter to inhibit both the hydrocarbon pool mechanism and formation of HCP precursors with the aim to obtain both high selectivity toward DME or stability overtime, respectively. In this concern, this work reports methanol conversion carried out at reaction temperature low enough (< 250 °C) to inhibit both hydrocarbon pool mechanism and olefins formation showing that catalyst structure affect strongly coke deposition and deactivation even when only DME is detected as product in reactor out-stream. In this sense, FER-type and MFI-type structure disclosed reliable shape-selectivity towards DME synthesis although more details about the role of acid sites should be better elucidate [27, 29, 37, 40].

Concerning the one-pot CO<sub>2</sub> hydrogenation to DME, the current research is focusing on the development of new catalytic system for and efficient CO<sub>2</sub> activation with selective production of DME. Physical mixture of Cu-ZnO catalyst with zeolite is the simplest way to obtain a bi-functional catalyst for DME synthesis. Recent works showed that CZ-ZrO<sub>2</sub>/zeolites hybrid grains prepared via co-precipitation method exhibits higher activity even if further efforts are required in order to obtain reliable DME productivities for a future industrial application of this process [27]. Realizing a new catalyst with a high synergy between redox and acid function is a current challenge in this field. The perfect hybrid catalyst should offer a high copper

dispersion (a high copper surface area), an efficient cooperation between acid sites and metal sites, a high resistance to water and a high resistance to deactivation (e.g. sintering of metals, coke deposition).

Catalytic performances of zeolite-based multifunctional catalyst can be improved by substituting  $\text{Al}_2\text{O}_3$  with  $\text{ZrO}_2$  or  $\text{Ga}_2\text{O}_3$  suggesting that several parameters have yet to be assessed for catalyst optimization. Also, acid function properties can be tuned in order to improve catalytic performances of hybrid grain. For instance, zeolites crystal size plays an important role in syngas-to-DME process [41] but this aspect is not investigated for  $\text{CO}_2$ -to-DME process. Also new synthesis routes for bi-functional catalyst should be explored (e.g. core shell systems, use of hierarchical zeolites, tailored acid sites location) in order to improve catalytic activity and stability [22]. On the whole, several parameters need to be investigated with the aim to give new insights for the design and the optimization of new catalytic system for one-pot  $\text{CO}_2$  hydrogenation to DME. In particular, the role played by metal-acid sites cooperation is not totally clear.

In this paper, a step by step optimization of the catalyst for DME synthesis is reported. The effect of zeolite structure and acidity on methanol dehydration reaction step is assessed by comparing catalytic performances of FER- and MFI-type zeolites with different acidity. With this aim, zeolites with FER and MFI structures and different Si/Al ratio were synthesized and characterized by XRD,  $\text{N}_2$  isotherms adsorption/desorption,  $\text{NH}_3$ -TPD and FT-IR analysis. Methanol dehydration step was carried out in a lab-scale fixed bed reactor equipped with both mass flows and temperature controllers. Once the best catalyst for methanol dehydration has been identified, a multifunctional hybrid grain was prepared by oxalate co-precipitation of CuZnZr precursors over bare zeolite crystals. The metal/acidic multifunctional catalytic bed configuration was optimized aiming to investigate the role of metal/acid sites proximity on DME productivity during one-pot  $\text{CO}_2$ -to-DME process.

## 2. MATERIALS AND METHODS

### 2.1 Synthesis

In order to assess the effect of zeolite features on the DME synthesis, FER-type and MFI-type zeolites with acidity were synthesized. In particular, the acidity of each zeolite structure was varied adopting different Si/Al ratio for the synthesis, i.e. Si/Al equals to 10, 30 and 60 were adopted for FER-type zeolites and Si/Al equals to 15, 25 and 50 were adopted for MFI-type zeolites. In particular MFI-type zeolites with different acidity level were prepared using tetrapropyl ammonium bromide (TPABr) as structure directing agent (SDA) by starting from a gel with the following molar composition:  $10 \text{ Na}_2\text{O} - 8 \text{ TPABr} - 100 \text{ SiO}_2 - x \text{ Al}_2\text{O}_3 - 2000 \text{ H}_2\text{O}$ , where  $x=1, 2$  and  $3.3$  according to the expected Si/Al molar ratio of 15, 25 and 50, respectively. As an example, MFI-type zeolite with Si/Al=25 was prepared as it follows: 2.7 g of NaOH (Aldrich) were dissolved in 119 g of distilled water. After that, 1 g of aluminum hydroxide (Aldrich) and 7.1 g of tetrapropyl ammonium bromide (Aldrich) were added to the former solution. After that, 20 g of precipitated silica (Silica gel 60, Merck) was slowly added and the resulting gel was stirred at 300 rpm for 1 hour at room temperature. The synthesis gel was therefore

transferred in PTFE-lined stainless-steel autoclaves and kept in a static oven at  $175^\circ\text{C}$  for 5, 4 or 2 days for samples prepared with Si/Al equals to 15, 25 and 50, respectively.

The synthesis of FER-type zeolite with Si/Al=10 was performed with pyrrolidine (Py) as SDA by adopting the following gel synthesis molar composition:  $0.6 \text{ Py} - 0.080 \text{ Na}_2\text{O} - 0.05 \text{ Al}_2\text{O}_3 - 1 \text{ SiO}_2 - 20 \text{ H}_2\text{O}$ .

In a typical synthesis, 1.69 gr of sodium alluminate and 0.165 gr of NaOH were dissolved in 39.8 gr of distilled water. 6.3 gr of pyrrolidine (Aldrich) were added dropwise and the gel was stirred for 30 min. 22 gr of LUDOX AS40 were added dropwise and the gel was stirred for 1h. The crystallization was carried out in 90 mL PTFE-lined stainless steel autoclave in tumbling conditions at 20 rpm at  $175^\circ\text{C}$  for 72 h. Synthesis of FER with gel Si/Al=30 and 60, named FER(30) and FER(60), respectively, were prepared by using pyridine as SDA. FER(30) was synthesized by adopting the following molar synthesis gel composition:  $0.6 \text{ Pyridine} - 0.087 \text{ Na}_2\text{O} - 0.017 \text{ Al}_2\text{O}_3 - 1 \text{ SiO}_2 - 25 \text{ H}_2\text{O}$ .

In a typical synthesis procedure 1.48 gr of NaOH and 0.89 gr of sodium aluminate are dissolved in 127 gr of distilled water. Therefore, 5.41 gr of pyridine (Aldrich) is added dropwise and the solution. After 30 minutes, 17 gr of fumed silica (Aldrich) is added to the solution. The obtained pasty gel is homogenized using a spatula for 30 minutes. The crystallization was carried out in 150 mL PTFE-lined stainless-steel autoclave in tumbling conditions at 20 rpm at  $165^\circ\text{C}$  for 7 days.

Similar procedure is adopted to synthesize ferrierite with gel Si/Al of 60, by adopting the following gel molar composition:  $2 \text{ Pyridine} - 0.058 \text{ Na}_2\text{O} - 0.008 \text{ Al}_2\text{O}_3 - 1 \text{ SiO}_2 - 25 \text{ H}_2\text{O}$ .

The crystallization is performed at the same temperature of FER(30) but for 5 days.

All the crystallized samples were separated from mother liquor by vacuum filtration and washed with distilled water until neutral pH of filtrate was obtained. The solid was dried at  $80^\circ\text{C}$  for 8 h and calcined at  $550^\circ\text{C}$  in air flow with the aim to remove organic molecules. H-form sample was obtained via exchange with  $\text{NH}_4\text{Cl}$  solution and calcined again at  $550^\circ\text{C}$  in order to eliminate ammonia and to obtain catalyst in acid-form. The obtained H-catalysts were directly used for dimethyl ether synthesis via vapor-phase methanol dehydration. Multifunctional catalysts for one-pot  $\text{CO}_2$ -to-DME process was prepared via gel oxalate co-precipitation of CuZnZr nitrate (60/30/10 at. %) in ethanol solutions over H-form zeolite crystals aiming to obtain a hybrid single grain (SG) with CZZ/zeolite with a weight ratio of 1:1. More details about the adopted procedure are reported elsewhere [35]. Furthermore, "homogenous" physical mixtures (PM) constituted by a pre-synthesized CZZ catalyst and a selected zeolite with a weight ratio of 1:1 were also realized.

### 2.2 Characterization

All of investigated samples were characterized via XRD with APD 2000 Pro diffractometer with a  $\text{Cu K}\alpha$  radiation (40 kV, 30 mA) in the range  $2\theta=5^\circ-50^\circ$ . The morphology of investigated catalysts was evaluated with both scanning and transmission electron microscopy (SEM – FEI model Inspect, TEM- Philips CM12). Textural properties (e.g. total surface area, micropore volume) were estimated by performing  $\text{N}_2$  adsorption/desorption isotherms at 77 K with ASAP 2020 (Micromeritics) instrument. Both  $\text{NH}_3$ -TPD and

H<sub>2</sub>-TPR analyses were performed according to already published procedures [41].

### 2.3 Catalytic tests

Vapor-phase methanol dehydration was carried out over H-form zeolites in the temperature range 140-200 °C with a methanol weight hourly space velocity (WHSV) of 4.5 gMeOH-h<sup>-1</sup> gcat<sup>-1</sup>, in a lab-scale apparatus described elsewhere [40]. Before each catalytic test, the reactor was purged with nitrogen at 240 °C in order to remove moisture from the catalyst. The catalytic activity of investigated hybrid catalysts during one-pot CO<sub>2</sub>-to-DME hydrogenation reaction was investigated in a fixed-bed reactor at 260 °C and total pressure of 3.0 MPa with a gas hourly space velocity (GHSV) of 8,800 NL/h/gcat by feeding a mixture with a CO<sub>2</sub>/H<sub>2</sub>/N<sub>2</sub>=3/9/1 molar ratio. Prior to each test, the catalyst was reduced in situ at 300 °C for 1h under hydrogen flow at atmospheric pressure. For both the processes, reactor stream was analyzed by GC equipped with flame ionized detector (FID) and a thermal conductivity detector (TCD).

## 3. RESULTS AND DISCUSSIONS

### 3.1 Textural properties

X-ray powder diffraction patterns reported in Figure 1 reveal that all of synthesized zeolites exhibit high purity and neither amorphous nor other phases (e.g. quartz) are detected. Furthermore, the total absence of background in the range 20-30 2 theta suggests that prepared samples have also a high crystallinity. Moreover, both crystallinity and purity seem not be dependent on the aluminum content. After metal co-precipitation no change on both crystallinity and purity was observed but metal oxide peaks appear (not shown).

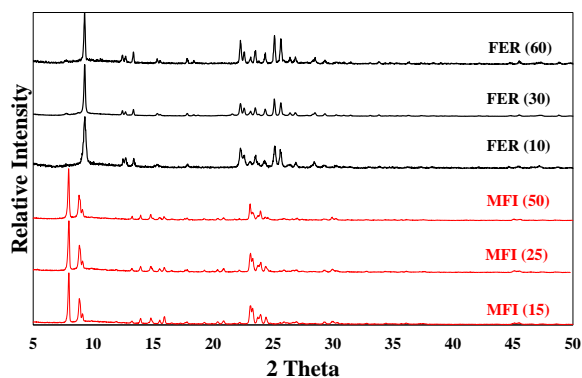


Figure 1. XRD of investigated FER- and MFI-type zeolites

N<sub>2</sub> adsorption isotherms carried out at 77 K are reported in Figure 2. For FER-type zeolite a type 1 isotherm is disclosed confirming the microporous structure of zeolites. In particular, FER(10) exhibits a higher nitrogen uptake than FER(30) and FER(60) indicating a higher surface area. Similar isotherms are also observed for MFI-type zeolites with no significant effect of aluminum content. On the other hand, a shoulder is present at P/P° around 0.2, typical of MFI-type channel system.

After metal co-precipitation nitrogen uptake strongly reduces and a mesoporosity is generated as revealed by the adsorption/desorption reported in Figure 3 for FER(10)-based catalysts. In fact, the hysteresis loop of FER(10) sample may

be related to the plate-like morphology of the crystals [35], that it is different from hysteresis loop observed for CZZ/FER(10) sample, indicating the generation of secondary mesoporosity that may be related to the metallic particles.

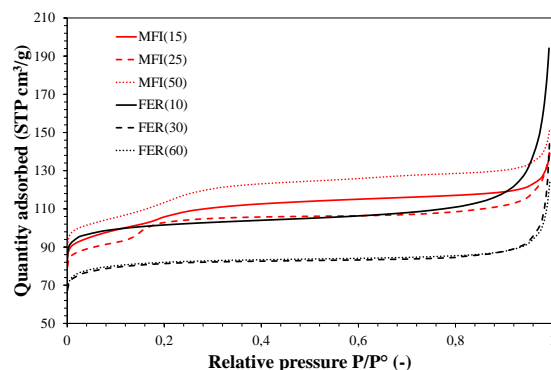


Figure 2. N<sub>2</sub> adsorption isotherms of investigated FER- and MFI-type zeolites

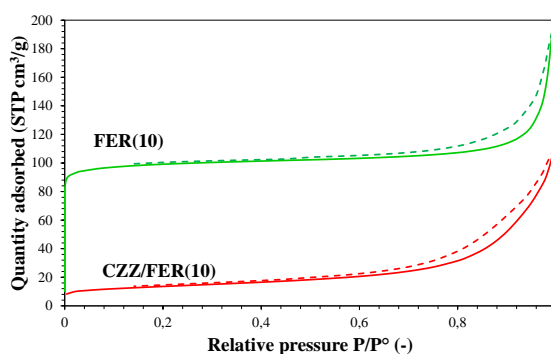


Figure 3. N<sub>2</sub> adsorption/desorption isotherms of FER(10) and CZZ/FER(10) sample

The main textural properties of the investigated materials are reported in Table 1. Both total surface area and micropore volume of bare zeolites are in agreement with the value reported in literature for similar materials. According to the isotherms previously discussed, FER(10) exhibits a B.E.T. surface area higher than FER(30) and FER(60), whilst the latter shows almost identical textural properties.

Table 1. Textural properties of investigated materials

Sample	Surface area <sup>1</sup> (m <sup>2</sup> /g)	Micropore volume <sup>2</sup> (cm <sup>3</sup> /g)	d <sub>Cu</sub> <sup>3</sup> (nm)
FER(10)	332	0.126	-
CZZ/FER(10)	217	0.052	4
FER (30)	272	0.108	-
FER (60)	275	0.110	-
MFI (15)	365	0.098	-
MFI(25)	360	0.118	-
MFI(50)	350	0.110	-
CZZ	162	-	11

1. Determined by Brunauer-Emmett-Teller equation

2. Determined by t-plot model

3. Cu average particle size determined by N<sub>2</sub>O chemisorption

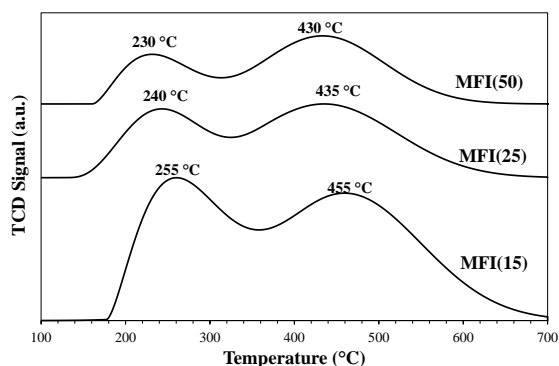
After co-precipitation of metals, both surfaces and micropore volume are strongly reduced, probably due to a partial pore blocking of zeolites due to the presence of CuCnZr particles. N<sub>2</sub>O measurements indicate that smaller copper particles are present on FER-type zeolite suggesting that there is some effect of the presence of zeolite on copper dispersion.

### 3.2 Acidity

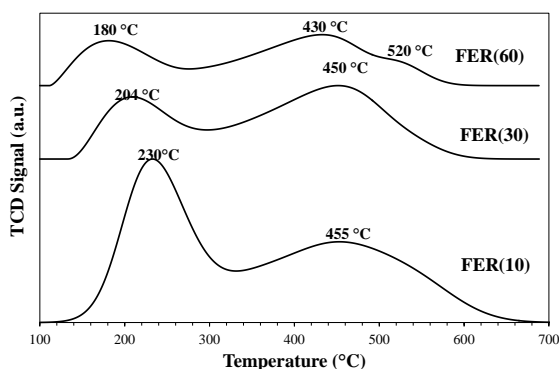
Figure 4 reports the ammonia-TPD profiles as a function of desorption temperature for MFI- and FER-type zeolites, respectively. NH<sub>3</sub>-TPD profiles allows to assess the strength of acid sites by relating weak acid sites to the ammonia desorbed in the temperature range 100-300 °C and strong acid sites to the ammonia desorbed at temperature higher than 300 °C. Furthermore, the temperature at which the maximum ammonia desorption occurs may be considered as a parameter of strength of acid sites, even if with same limitations [42]. As the NH<sub>3</sub>-TPD profiles show, both weak and acid sites are present for both MFI- and FER-type zeolite. For MFI-type zeolite the temperature of maximum ammonia desorption from weak acid sites (WT) increases as aluminum content increases (MFI(15)>MFI(25)>MFI(50) in the range 230-255 °C. Similar behavior is exhibited by FER-type zeolites, but WT is in the range 180-230 °C indicating that FER-type zeolites exhibit weaker acid sites than MFI-type zeolite. On the contrary, both FER- and MFI-type zeolites exhibit similar strength of strong acid sites. Also, for strong acid sites, the maximum temperature of ammonia desorption increases by increasing the aluminum content, passing from 430 °C to 455 °C. It is important to note a broad band at about 520 °C for FER(60) sample indicating the presence of a third acid site type with a higher strength.

Table 2 reports the acidity of investigated samples. Considering bare zeolites, total acidity increases accordingly with aluminum content.

In particular, a linear relationship was found between total acidity and Si/Al ratio for MFI-type zeolites and FER(30) and FER(60) zeolites as reported in Figure 5.



(a) NH<sub>3</sub>-TPD profiles of MFI-type zeolites



(b) NH<sub>3</sub>-TPD profiles of FER-type zeolites

**Figure 4.** NH<sub>3</sub>-TPD profiles of MFI-type and FER-type zeolites

**Table 2.** Acidity properties of investigated materials

Sample	Total acidity <sup>1</sup> ( $\mu\text{mol/g}$ )	Weak acid fraction (-)	Strong acid fraction (-)
FER(10)	790	0.35	0.65
CZZ/FER(10)	500	0.28	0.72
FER (30)	480	0.14	0.86
FER (60)	330	0.10	0.90
MFI (15)	602	0.45	0.55
MFI(25)	515	0.42	0.58
MFI(50)	354	0.45	0.55

1. Determined from desorbed NH<sub>3</sub> in the temperature range 100-700 °C

2. Determined from desorbed NH<sub>3</sub> in the temperature range 100-300 °C

3. Determined from desorbed NH<sub>3</sub> in the temperature range 300-700 °C

On the contrary, FER(10) seems to not follows this trend and it may be related to the presence of large amount of defects (i.e. silanols) may be responsible of part of measured weak acidity [35].

Furthermore, MFI-type zeolites disclose a similar fraction of weak (about 45 %) and strong sites (about 55 %). Similar distribution was observed for FER(10).

On the contrary, both FER(30) and FER(60) disclose a higher fraction of strong acid sites (more than 85 %).

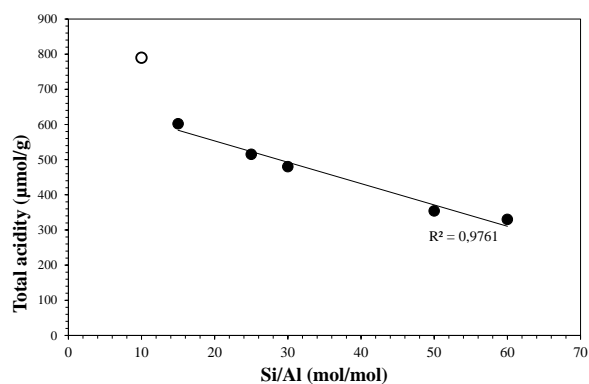


**Figure 5.** Total acidity as a function of Si/Al molar ratio

FT-IR analysis (not shown) carried out with both carbon monoxide and D<sub>3</sub>-acetonitrile reveals that only FER(10) possesses Lewis acid sites with a Lewis/Brønsted ratio equals to 0.33, whilst mainly Brønsted acid sites are present on the other FER- and MFI-type samples.

### 3.3 MeOH-to-DME

Methanol conversion as a function of reaction temperature in the range 140-200 °C for all of investigated zeolites is reported in Figure 6. In the entire range of temperature only DME was observed with no formation of by-products. Such as olefins or other hydrocarbons.

Methanol conversion increases as the temperature increases according to the Arrhenius's trend as reported in Figure 7.

Apparent activation energies ( $E_{app}$ ) are then calculated and results are reported in Table 3.  $E_{app}$  values indicate that the activation barrier is always lower for FER-type materials and it decreases as the total acidity increases. Similar trend was followed by MFI-type zeolites.

FER(10) zeolite shows the highest activity in terms of methanol conversion, approaching to the theoretical thermodynamic equilibrium value at the 200 °C.

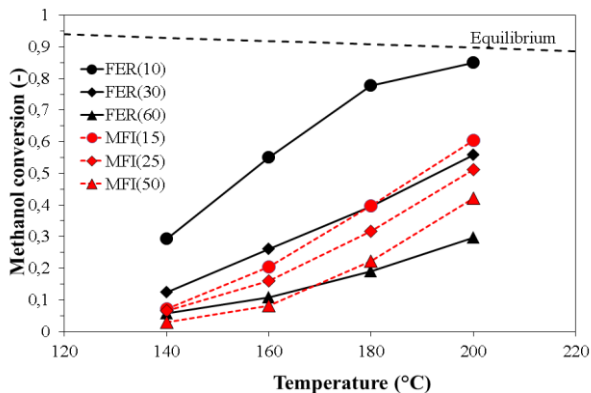


**Figure 6.** Methanol conversion as a function of reaction temperature for the investigated H-zeolites

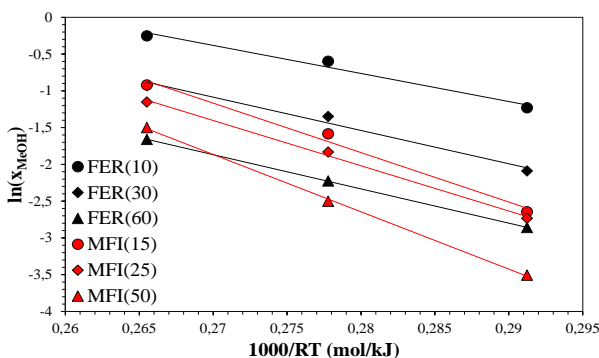


**Figure 7.** Arrhenius plot

**Table 3.** Apparent activation energies calculated from Arrhenius plot reported in Figure 8

Sample	Fitting linear equation*	R <sup>2</sup>	Apparent activation energy (kJ/mol)
FER(10)	y=-38x+9.9	0.980	38
FER(30)	y=-45x+11.1	0.983	45
FER(60)	y=-47x+10.7	1.000	47
MFI(15)	y=-58x+17.1	0.998	58
MFI(25)	y=-62x+15.2	0.998	62
MFI(50)	y=-78x+19.2	0.999	78

Note:  $y = \ln(\text{methanol conversion})$ ;  $x = 1000/RT$ ,  $R = 8.314 \text{ J/molK}$ ,  $T = \text{temperature expressed in K}$ .

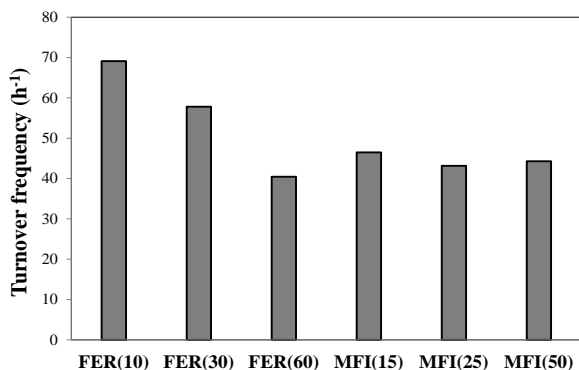


**Figure 8.** Turnover frequency of methanol-to-dimethyl ether reaction calculated at 180 °C

On the whole, results indicate that catalytic activity during methanol dehydration to DME reaction strongly depends on

the acidity of zeolite. In fact, methanol conversion follows the order FER(10)>FER(30)>FER(60) for FER-type zeolites and MFI(15)>MFI(25)>MFI(50) for MFI-type zeolites. On the other hand, although MFI(15) possesses a higher concentration of total acid sites, it shows a lower activity than FER(30) especially at low temperature. Similar behavior is also disclosed for FER(60) and MFI(50) samples. A different trend is observed at temperature higher than 180 °C as both MFI(15) and MFI(50) exhibit a higher activity than FER(30) and FER(60), respectively.

Such behavior may be related to weak/strong acid sites distribution. In fact, the activity order seems to follow strong acid sites concentration at lower temperature and total acid sites concentrations at higher temperature. In fact, it is reasonable to conclude that mainly strong acid sites are active at lower temperature, whilst weak acid sites became able to catalyze the dehydration of methanol at temperature above or equals to 180 °C. At this temperature turnover frequency may be then calculated and results are reported in Figure 8. Turnover frequency follows the order

FER(10)>FER(30)>MFI(15)>MFI(50)>MFI(25)>FER(60) revealing that FER(10) and MFI(15) are the most efficient catalysts among the FER-type and MFI-type zeolites, respectively.

### 3.4 CO<sub>2</sub>-to-DME

As reported in the previous paragraph, FER(10) may be considered as the most active catalyst for methanol dehydration reaction step, among the investigated FER-type and MFI-type zeolites, respectively. Therefore, one-pot CO<sub>2</sub>-to-DME reaction was carried out at 260 °C and 30 bar by using FER(10) as acid catalyst in three different multifunctional catalytic bed configurations: CZZ-FER(10) dual bed (DB), physical mixture (PM) and hybrid single grain (SG). Figure 9 reports the results of catalytic tests under one-pot CO<sub>2</sub> hydrogenation to DME conditions.

CO<sub>2</sub> conversion is about 18 % for DB system, and it increases at 20 and 22 % for PM and SG systems, respectively. Catalytic tests carried out over CZZ reveal a similar CO<sub>2</sub> conversion and CO selectivity observed for DB system, suggesting that no significant catalytic improvement is obtained when a dual bed is used, highlighting the importance to have an intrinsic cooperation between metallic and acid sites.

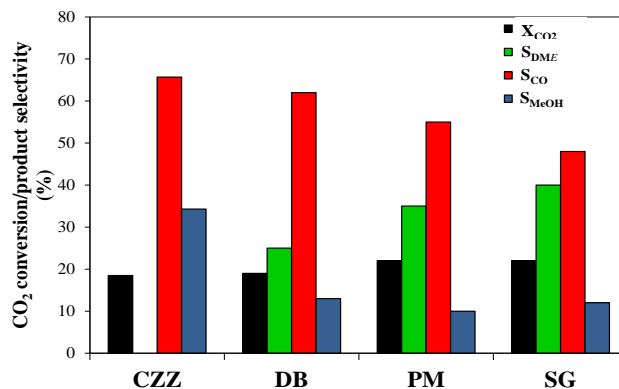


**Figure 9.** CO<sub>2</sub> conversion and selectivity towards DME (S<sub>DME</sub>), CO (S<sub>CO</sub>) and methanol (S<sub>MeOH</sub>) for the investigated CZZ/FER(10)-DB, -PM and -SG systems and CZZ catalyst (T<sub>R</sub>: 260 °C, P<sub>R</sub>: 30 bar, GHSV: 8800 NL/h/g<sub>cat</sub>)

Moreover, reactor bed configuration also strongly affects product distribution.

DME selectivity is lower for dual bed reactor that exhibits a DME selectivity of 25 %, meaning that only 5 % of carbon is converted into dimethyl ether. DME selectivity is increased up to 35 % when both CZZ and FER(10) powders are “homogenously” mixed.

When hybrid single grain is used, catalytic performances are further improved, leading to a DME selectivity of 40 %, meaning that more than 10 % of carbon is converted towards the desired product. Such result clearly shows that the efficiency of catalytic bed strongly depends on the possibility to have an intimate interaction between metallic and acid sites. In that sense, hybrid single grain system facilitates the mass transfer between the sites, so promoting a more rapid dehydration of methanol towards dimethyl ether, and brings out the thermodynamic advantages of one-pot process. Therefore, the efficiency of one-pot process is not only related to have the possibility to carried out the reaction in the same reactor unit but also to have a catalytic system with an intimate interaction between the active sites involved in the process.

On the whole, the space-time yield calculated for the investigated system was 732, 640 and 395  $\text{g}_{\text{DME}}/\text{h}/\text{kg}_{\text{cat}}$  for SG, PM and DB systems, respectively, again highlighting the crucial role of metal-acid proximity in the synthesis of dimethyl ether. Nevertheless, a gradual deactivation is also observed. In particular, for SG both  $\text{CO}_2$  conversion and DME selectivity decreases with the time, and after about 40 h time-on-stream the DME productivity is about 380  $\text{g}_{\text{DME}}/\text{h}/\text{kg}_{\text{cat}}$ . Surprisingly, a higher stability is exhibited by PM system with a final DME productivity of about 450  $\text{g}_{\text{DME}}/\text{h}/\text{kg}_{\text{cat}}$ . This behavior may be related to some aspects involving metal/acid proximity. For instance, it may be due to  $\text{Cu}^+/\text{H}^+$  ion exchange or metal sintering promoted by water on zeolite surface.

#### 4. CONCLUSIONS

In this work, FER-type and MFI-type zeolites with different acidity were used as catalysts for DME synthesis via both methanol dehydration and one-pot  $\text{CO}_2$  hydrogenation. Both zeolite structure and acidity strongly affect catalysis of methanol dehydration. In particular, methanol conversion increases as the acidity increases but the presence of Lewis acid sites seems to favor the reaction. On the whole FER-type zeolite with  $\text{Si}/\text{Al}=10$ , named FER(10), exhibits the best performances in terms of DME turnover frequency. Therefore, FER(10) zeolite was also used as acid catalyst for one-pot  $\text{CO}_2$  hydrogenation to DME coupled with  $\text{CuZnZr}$  (CZZ) metallic system. Among several catalytic bed configurations assessed (i.e. dual bed, physical mixture and hybrid single grain), the dual bed reactor resulted to be the less effective configuration, whilst hybrid single grain prepared via gel-oxalate co-precipitation of metal precursors over zeolite crystals exhibited significant better catalytic performance, with a DME productivity of  $732\text{g}_{\text{DME}}/\text{h}/\text{kg}_{\text{cat}}$ , almost doubled than that obtained with double bed configuration. A gradual catalyst deactivation was observed and different phenomena may be the cause of such behavior and further investigation are being performed in order to elucidate that aspect. In particular, future works should be devoted to the study of new multifunctional catalytic systems

designed with the aim to improve the cooperation between metal and acid sites but taking into account the role played by mobility of metal particles on the stability. Both sintering and  $\text{Cu}^+/\text{H}^+$  ion exchange seems to be the main cause of deactivation of current catalysts during one pot  $\text{CO}_2$ -to-DME process and such aspects need to be better investigated. The onsite water removal (e.g. with membrane reactor) even is a future scenario to be explored.

#### REFERENCES

- [1] Catizzone, E., Bonura, G., Migliori, M., Braccio, G., Frusteri, F., Giordano, G. (2019). The effect of zeolite features on catalytic performances of  $\text{CuZnZr}/\text{zeolite}$  hybrid catalysts in one-pot  $\text{CO}_2$ -to-DME hydrogenation. *Tecnica Italiana - Italian J. Eng. Sci.*, 63(2-4): 257-262. <https://doi.org/10.18280/ti-ijes.632-420>
- [2] Olah, G.A. (2005). Beyond oil and gas: The methanol economy. *Angew. Chem. Int. Ed.*, 44(18): 2636-2639. <https://doi.org/10.1002/anie.200462121>
- [3] Wood, D.A., Nwaoha, C., Towler, B.F. (2012). Gas-to-liquids (GTL): A review of an industr offering several routes for monetizing natural gas. *J. Nat. Gas Sci. Eng.*, 9: 196-208. <https://doi.org/10.1016/j.jngse.2012.07.001>
- [4] Aasberg-Petersen, K., Hansen, J.-H.B., Christensen, T.S., Dybkjaer, I., Christensen, P.S., Nielsen, C.S., Madsen, S.E.L.W., Rostrup-Nielsen, J.R. (2001). Technologies for large-scale gas conversion. *Appl. Catal. A*, 221(1-2): 379-387. [https://doi.org/10.1016/S0926-860X\(01\)00811-0](https://doi.org/10.1016/S0926-860X(01)00811-0)
- [5] Perathoner, S., Centi, G. (2014).  $\text{CO}_2$  recycling: A key strategy to introduce green energy in the chemical production chain. *ChemSusChem*, 7(5): 1274-1282. <https://doi.org/10.1002/cssc.201300926>
- [6] Molino, A., Migliori, M., Blasi, A., Davoli, M., Marino, T., Chianese, S., Catizzone, E., Giordano, G. (2017). Municipal waste leachate coconversion via catalytic supercritical water gasification process. *Fuel*, 206: 155-151, 2017. <https://doi.org/10.1016/j.fuel.2017.05.091>
- [7] Arcoumanis, C., Bae, C., Crookes, R., Kinoshita, E. (2008). The potential of di-methyl ether (DME) as an alternative fuel for compression-ignition engines: A review. *Fuel*, 87(7): 1014-1030. <https://doi.org/10.1016/j.fuel.2007.06.007>
- [8] Park, S.H., Lee, C.S. (2014). Applicability of diemthyl ether (DME) in a compression ignition engine as an alternative fuel. *Energ. Conv. Manag.*, 86: 848-863. <https://doi.org/10.1016/j.enconman.2014.06.051>
- [9] Semelsberg, T.A., Borup, R.L., Greene, H.L. (2006). Dimethyl ether (DME) as an alternative fuel. *J. Power Sourc.*, 156(2): 497-511. <https://doi.org/10.1016/j.jpowsour.2005.05.082>
- [10] Azizi, Z., Rezaeimanesh, M., Tohidian, T., Rahimpour, M.R. (2014). Dimethyl ether: A review of technologies and production challenges. *Chem. Eng. Process. Proc. Int.*, 82: 150-172. <https://doi.org/10.1016/j.cep.2014.06.007>
- [11] Sun, J., Yang, G., Yoneyama, Y., Tsubaki, N. (2014). Catalysis chemistry of dimethyl ether synthesis. *ACS Catal.*, 4(10): 3346-3356. <https://doi.org/10.1021/cs500967j>
- [12] Yoon, E.S., Han, C. (2009). A review of sustainable energy - recent development and future prospects of

- dimethyl ether (DME). *Comp. Aid. Chem. Eng.*, 27: 169-175. [https://doi.org/10.1016/S1570-7946\(09\)70249-4](https://doi.org/10.1016/S1570-7946(09)70249-4)
- [13] Graves, C., Ebbesen, S.D., Mogensen, M., Lackner, K.S. (2011). Sustainable hydrocarbon fuels by recycling CO<sub>2</sub> and H<sub>2</sub>O with renewable or nuclear energy. *Renew. Sus. Energ. Rev.*, 15(1): 1-23. <https://doi.org/10.1016/j.rser.2010.07.014>
- [14] Aresta, M., Dibenedetto, A., Angelini, A. (2013) The changing paradigm in CO<sub>2</sub> utilization. *J. CO<sub>2</sub> Util.*, 3-4: 65-73. <https://doi.org/10.1016/j.jcou.2013.08.001>
- [15] Jia, G., Tan, Y., Han, Y. (2006). A comparative study on the thermodynamics of dimethyl ether synthesis from CO hydrogenation and CO<sub>2</sub> hydrogenation. *Ind. Eng. Chem. Res.*, 45(3): 1152-1159. <https://doi.org/10.1021/ie050499b>
- [16] An, X., Zuo, Y.-Z., Zhang, Q., Wang, D., Wang, J.-F. (2008). Dimethyl ether synthesis from CO<sub>2</sub> hydrogenation on a CuO-ZnO-Al<sub>2</sub>O<sub>3</sub>-ZrO<sub>2</sub>/HZSM-5 bifunctional catalyst. *Ind. Eng. Chem. Res.*, 47(17): 6547-6554. <https://doi.org/10.1021/ie800777t>
- [17] Bourzutschky, J.A., Homs, N., Bell, A.T. (1990). Hydrogenation of CO<sub>2</sub> and CO<sub>2</sub>/CO mixtures over copper-containing catalysts. *J. Catal.*, 124(1): 73-85. [https://doi.org/10.1016/0021-9517\(90\)90104-R](https://doi.org/10.1016/0021-9517(90)90104-R)
- [18] Brown, D.M., Bhatt, B.L., Hsiung, T.H., Lewnard, J.J., Waller, F.J. (1991). Novel technology for the synthesis of dimethyl ether from syngas. *Catal. Today*, 8(3): 279-304. [https://doi.org/10.1016/0920-5861\(91\)80055-E](https://doi.org/10.1016/0920-5861(91)80055-E)
- [19] Olah, G.A., Goepfert, A., Prakash, G.K. (2009). Chemical recycling of carbon dioxide to methanol and dimethyl ether: from greenhouse gas to renewable, environmentally carbon neutral fuels and synthetic hydrocarbons. *J. Org. Chem.*, 74(2): 487-498. <https://doi.org/10.1021/jo801260f>
- [20] Li, Y., Wang, T., Yin X., Wu, C., Ma, L., Li, H., Lv, Y., Sun, L. (2010). 100 t/a-scale demonstration of direct dimethyl ether synthesis from corn-cob-derived syngas. *Ren. Energ.*, 35(3): 583-587. <https://doi.org/10.1016/j.renene.2009.08.002>
- [21] Ge, Q., Huang, Y., Qiu, F., Li, S. (1998). Bifunctional catalysts for conversion of synthesis gas to dimethyl ether. *Appl. Catal. A: Gen.*, 167(1): 23-30. [https://doi.org/10.1016/S0926-860X\(97\)00290-1](https://doi.org/10.1016/S0926-860X(97)00290-1)
- [22] Catizzone, E., Bonura, G., Migliori, M., Frusteri, F., Giordano, G. (2018). CO<sub>2</sub> recycling to dimethyl ether: State-of-the-art and perspectives. *Molecules*, 23(1): 31-58. <https://doi.org/10.3390/molecules23010031>
- [23] Sierra, I. Erena, J., Aguayo, T., Olazar, M., Bilbao, J. (2010). Deactivation kinetics for direct dimethyl ether synthesis on a CuO-ZnO-Al<sub>2</sub>O<sub>3</sub>/γ-Al<sub>2</sub>O<sub>3</sub> catalysts. *Ind. Eng. Chem. Res.*, 49(2): 481-489. <https://doi.org/10.1021/ie900978a>
- [24] Naik, S.P., Ryu, T., Bui, V., Miller, J.D., Drinnan, N., Zmierzak, W. (2011). Synthesis of DME from CO<sub>2</sub>/H<sub>2</sub> gas mixture. *Chem. Eng. J.*, 167(1): 362-368. <https://doi.org/10.1016/j.cej.2010.12.087>
- [25] Abu-Dahrieh, J., Rooney, D., Goguet, A., Saih, Y. (2012). Activity and deactivation studies for direct dimethyl ether synthesis using CuO-ZnO-Al<sub>2</sub>O<sub>3</sub> with NH<sub>4</sub>ZSM-5, HZSM-5 or γ-Al<sub>2</sub>O<sub>3</sub>. *Chem. Eng. J.*, 203(1): 201-211. <https://doi.org/10.1016/j.cej.2012.07.011>
- [26] Bonura, G., Migliori, M., Frusteri, L., Cannilla, C., Catizzone, E., Giordano, G., Frusteri, F. (2018). Acidity control of zeolite functionality on activity and stability of hybrid catalysts during DME production via CO<sub>2</sub> hydrogenation. *J. CO<sub>2</sub> Util.*, 24: 398-406. <https://doi.org/10.1016/j.jcou.2018.01.028>
- [27] Bonura, G., Frusteri, F., Cannilla, C., DragoFerrante, G., Aloise, A., Catizzone E., Migliori, M., Giordano, G. (2016). Catalytic features of CuZnZr-zeolite hybrid systems for the direct CO<sub>2</sub>-to-DME hydrogenation reaction. *Catal. Today*, 277: 48-54. <https://doi.org/10.1016/j.cattod.2016.02.013>
- [28] Catizzone, E., Migliori, M., Purita, A., Giordano, G. (2019). Ferrierite vs. γ-Al<sub>2</sub>O<sub>3</sub>: the superiority of zeolites in terms of water-resistance in vapour-phase dehydration of methanol to dimethyl ether. *J. Energ. Chem.*, 30: 162-169. <https://doi.org/10.1016/j.jechem.2018.05.004>
- [29] Migliori, M., Catizzone, E., Aloise, A., Bonura, G., Gomez-Hortiguera, L., Frusteri, L., Cannilla, C., Frusteri, F., Giordano, G. (2018). New insights about coke deposition in methanol-to-DME reaction over MOR-, MFI- and FER-type zeolites. *J. Ind. Eng. Chem.*, 68: 196-208. <https://doi.org/10.1016/j.jiec.2018.07.046>
- [30] Guisnet, M., Magnoux, P. (1989). Coking and deactivation of zeolites: influence of the pore structure. *Appl. Catal.*, 54(1): 1-27. [https://doi.org/10.1016/S0166-9834\(00\)82350-7](https://doi.org/10.1016/S0166-9834(00)82350-7)
- [31] Derouane, E.G. (1985). Factor affecting the deactivation of zeolites by coking. *Stud. Surf. Sci. Catal.*, 20: 221-240. [https://doi.org/10.1016/S0167-2991\(09\)60173-7](https://doi.org/10.1016/S0167-2991(09)60173-7)
- [32] Corma, A. (1995). Inorganic solid acids and their use in acid-catalyzed hydrocarbon reactions. *Chem. Rev.*, 95: 559-614. <https://doi.org/10.1021/cr00035a006>
- [33] Corma, A. (2003). State of the art and future challenges of zeolites as catalysts. *J. Catal.*, 216(1-2): 298-312. [https://doi.org/10.1016/S0021-9517\(02\)00132-X](https://doi.org/10.1016/S0021-9517(02)00132-X)
- [34] Catizzone, E., Migliori, M., Aloise, A., Lamberti, R., Giordano, G. (2019). Hierarchical low Si/Al ratio ferrierite zeolite by sequential postsynthesis treatment: catalytic assessment in dehydration reaction of methanol. *J. Chem.*, <https://doi.org/10.1155/2019/3084356>
- [35] Catizzone, E., Van Daele, S., Bianco, M., Di Michele, A., Aloise, A., Migliori, M., Valtchev, V., Giordano, G. (2019). Catalytic application of ferrierite nanocrystals in vapour-phase dehydration of methanol to dimethyl ether. *Appl. Catal. B: Env.*, 243: 273-282. <https://doi.org/10.1016/j.apcatb.2018.10.060>
- [36] Prasad, P.S., Bac, J.W., Kang, S.-H., Lee, Y.-J., Jun, K.-W. (2008). Single-step synthesis of DME from syngas on Cu-ZnO-Al<sub>2</sub>O<sub>3</sub>/zeolite bifunctional catalysts: The superiority of ferrierite over the other zeolites. *Fuel Process. Technol.*, 89(12): 1281-1286. <https://doi.org/10.1016/j.fuproc.2008.07.014>
- [37] Catizzone, E., Aloise, A., Migliori, M., Giordano, G. (2017). From 1-D to 3-D zeolite structures: performance assessment in catalysis of vapour-phase methanol dehydration to DME. *Microp. Mesopo. Mater.*, 243: 102-111. <https://doi.org/10.1016/j.micromeso.2017.02.022>
- [38] Centi, G., Perathoner, S., Pino, F., Arrigo, R., Giordano, G., Katovic, A., Pedulà, V. (2005). Performances of Fe-[Al, B]MFI catalysts in benzene hydroxylation with N<sub>2</sub>O: The role of zeolite defects as host sites for highly

- active iron species. *Catal. Today*, 110(3-4): 211-220. <https://doi.org/10.1016/j.cattod.2005.09.041>
- [39] Campelo, J.M., Lafont, F., Marinas, J.M., Ojeda, M. (2000). Studies of catalyst deactivation in methanol conversion with high, medium and small pore silicoaluminophosphates. *Appl. Catal. A.*, 192(1): 85-96. [https://doi.org/10.1016/S0926-860X\(99\)00329-4](https://doi.org/10.1016/S0926-860X(99)00329-4)
- [40] Bonura, G., Cannilla, C., Frusteri, L., Mezzapica, A., Frusteri, F. (2017). DME production by CO<sub>2</sub> hydrogenation: key factors affecting the behaviour of CuZnZr/ferrierite catalysts. *Catal. Today*, 281(1): 337-344. <https://doi.org/10.1016/j.cattod.2016.05.057>
- [41] Ordonsky, V.V., Cai, M., Sushkevich, V., Moldovan, S., Ersen, O., Lancelot, C., Valtchev, V., Khodakov, A.Y. (2014). The role of external acid sites of ZSM-5 in deactivation of hybrid CuZnAl/ZSM-5 catalyst for direct dimethyl ether synthesis from syngas. *Appl. Catal. A: Gen.*, 486: 266-275. <https://doi.org/10.1016/j.apcata.2014.08.030>
- [42] Niwa, M., Katada, N. (2013). New method for the temperature-programmed desorption (TPD) of ammonia experiment for characterization of zeolite acidity: A review. *The Chemical Record*, 13(5): 432-455. <https://doi.org/10.1002/tcr.201300009>